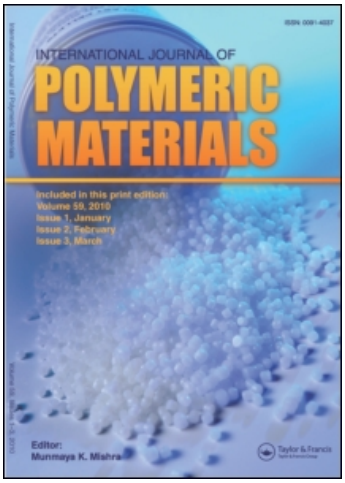

International Journal of Polymeric Materials
Publication details, including instructions for authors and subscription information:
http://www.informaworld.com/smpp/title~content=t713647664

Uniaxial extension of poly(diethylsiloxane) networks: Mesophase formation under stress

V. Papkov[a]; A. Turetski[a]; Geradus. J. Out[b]; Martin Möller[b]
[a] A. N. Nesmjanov Institute of Organo-Element Compounds, Russian Academy of Sciences, Moscow, Russia [b] Laboratory for Organic and Macromolecular Chemistry, OCIII University of Ulm, Germany

Online publication date: 27 October 2010

To cite this Article Papkov, V. , Turetski, A. , Out, Geradus. J. and Möller, Martin(2002) 'Uniaxial extension of poly(diethylsiloxane) networks: Mesophase formation under stress', International Journal of Polymeric Materials, 51: 4, 369 — 391
To link to this Article: DOI: 10.1080/00914030214762
URL: http://dx.doi.org/10.1080/00914030214762

International Journal of Polymeric Materials, 51:369–391, 2002

0091-4037/02 $12.00 + .00

UNIAXIAL EXTENSION OF POLY(DIETHYLSILOXANE) NETWORKS: MESOPHASE FORMATION UNDER STRESS

V. Papkov and A. Turetski
A. N. Nesmjanov Institute of Organo-Element Compounds, Russian Academy of Sciences, Moscow, Russia

Geradus. J. Out and Martin Möller
Laboratory for Organic and Macromolecular Chemistry, OCIII
University of Ulm, Germany

The mesophase formation in chemically well-defined poly(diethylsiloxane) [PDES] networks has been investigated upon uniaxial extension by means of stress–strain and birefringence measurements. Variation of the temperature range of the mesomorphic state was shown to depend on the molecular weight between crosslinks, M_c, and the applied stress. Formation and behavior of mesocrystals under stress can be described qualitatively within the framework of the crystallization thermodynamics and kinetics in stretched rubber. A particular feature of the mesophase formation in PDES networks under stress is that, at the initial stage of extension, metastable mesocrystals form with sizes smaller than M_c that can reorganize on further extension into larger crystallites with a longitudinal size and isotropization temperature that is determined by M_c. This transformation process is the cause of a peculiar stress–strain behavior of PDES networks on extension and subsequent contraction.

Keywords: poly(diethylsiloxane), networks, liquid-crystal, mesophase

INTRODUCTION

Poly(diethylsiloxane), PDES, is a symmetrically substituted organo-element polymer, that transforms above 290° K from the crystalline phases α_2 and β_2 into a thermotropic mesophase [1, 2] also referred to as columnar mesophase

Received 12 September 2000.
The present address of Geradus. J. Out is DSM Research, Geleen, The Netherlands.
The authors thank cordially Dr. V. Vasiliev for the indentation experiments. Financial support was granted by the Russian Foundation for Fundamental Sciences (grant no. 98-03-33329) and the Deutsche Forschungsgemeinschaft (Teilprojekt F4, SFB 239).
Address correspondence to V. Papkov, A. N. Nesmjanov Institute of Organo-Element Compounds, Russian Academy of Sciences, Ulitsa Vavilova 28, CSP 1, 117334 Moscow, Russia. E-mail: vspapk@ineos.ac.ru

[3, 4]. PDES possesses a relatively low isotropization temperature $T_i \cong 326\,K$. Crosslinked PDES can undergo large reversible deformations in the amorphous state due to a high flexibility of the macromolecules [2, 5, 6]. Crosslinking of linear PDES increases the amorphous phase content and decreases T_i. Mechanical stress applied to amorphous PDES networks was found to induce formation of the mesophase and to increase T_i. It has been proposed that this process obeys the thermodynamic relationships describing crystallization of elastomers under stress [5]. However, while the increase of the melting point of crystallizable elastomers does usually not exceed $10-20\,K$ upon stretching, T_i of constrained PDES networks can rise much more (even by $\sim 100\,K$) [7].

Depending on the crosslink density and the stress applied, PDES networks can behave either as plastic materials or as rubbers in a wide temperature range. This variability in properties of PDES networks motivate a systematic study on the influence of the network topology on their phase and mechanical behavior. We have reported the synthesis of PDES networks with well-defined network strands M_c between crosslinks and their phase behavior in quiescent state [8]. Also some preliminary data on the mechanical properties of these networks were published earlier [9]. The objective of the present paper is a detailed consideration of the mesophase formation upon uniaxial extension of the PDES networks, mainly based on the results of stress–strain and birefringence measurements.

EXPERIMENTAL

Materials

PDES networks were prepared by means of hydrosilylation cross-linking of well-defined poly(diethylsiloxane) telechelics (with vinyl and allyl endgroups) of various molecular weights with relatively narrow molecular weight distributions using a multifunctional Si—H cross-linking agent with a functionality equal to 8 in excess, providing an expected average functionality of the crosslinks equal to 5.3. We used such a multifunctional cross-linking agent in order to produce PDES networks with proper tensile strengths. The synthesis of the initial telechelics, their molecular weight parameters, the crosslinking procedure and some characteristics of the networks (sol fraction, equilibrium swelling, the temperatures and heats of phase transitions) are described in detail elsewhere [8]. M_c of the networks was nominally taken equal to the number-average molecular weight (MW) of the telechelics. Four unimodal networks with M_c equal to $22{,}000\,g\,mol^{-1}$ (PDES-22), $56{,}000\,g\,mol^{-1}$ (PDES-56), 94,000 (PDES-94) and $115000\,g\,mol^{-1}$ (PDES-115) and two bimodal ones, PDES-9 m (90 w.% of $M_c = 56{,}000\,g\,mol^{-1}$; 10 w.% of $M_c = 22{,}000\,g\,mol^{-1}$; averaged $M_c = 49{,}000$) and PDES-5 m

(50 w.% of $M_c = 56{,}000\,\mathrm{g\,mol^{-1}}$; 50 w.% of $M_c = 22{,}000\,\mathrm{g\,mol^{-1}}$; averaged $M_c = 32{,}000$), were the subject of our investigation.

Methods

Stress–strain measurements in the mode of uniaxial extension were made on a home-built apparatus that permitted to monitor simultaneously stress and birefringence as functions of strain at various temperatures [10, 11]. A polarization modulation technique was used to determine the birefringence. The beam of a HeNe-laser operating at a wavelength of 633 nm passed subsequently through a linear polarizer, the sample, a quarter wave plate and finally a rotating polarizer to the detector. The temperature was held with an accuracy of ± 1 K. Stress–strain curves were taken at strain rates of 0.5, 0.1 and $0.005\,\mathrm{min^{-1}}$ using rectangular samples of $20 \times 5 \times 1$ mm in size. In order to determine T_i of the mesocrystals in constrained oriented PDES networks, stress relaxation was monitored upon heating with a rate of 2 K/min.

The initial modulus of elasticity E of the amorphous networks was obtained according to the Hertz equation using the ball indentation method [12]:

$$E = 3(1 - \nu^2)F/4r^{1/2}h^{3/2} \tag{1}$$

where F represents the force by which a sphere is pressed against the surface of a network sample, r is the radius of the sphere, h is the depth of indentation of sphere and μ represents Poisson's ratio that has been taken equal 0.5. All experiments were carried out with a home-made device ($r = 0.15$ cm, h varied in a range of $5\ 10^{-3}$–$2\ 10^{-2}$ cm was measured with an accuracy of $2\ 10^{-4}$ cm).

X-ray diffraction pattern were obtained using Ni-filtered CuKα radiation. Temperature dependent diffractograms were recorded on a circular film with a radius of 57.3 mm using a Guinier-Simon camera. Optical density data were collected from the photographically obtained pattern using a LS20 linear micro densitometer controlled by SCANPI software. First the diffractograms were taken at ambient temperature and then on heating and subsequent cooling. Prior to measurements, the samples were annealed at the required temperature for 30 min. Exposure times were about 3 hours. Temperature-dependent X-ray diffractograms of strained, previously highly oriented mesomorphic PDES networks were taken with a DRON-2 diffractometer (Russia) provided with a special temperature cell at a heating rate of 2 K/min.

Differential scanning calorimetry (DSC) traces presented in the article reproduce our data published earlier [8]. They were taken with a

Perkin-Elmer DSC-2, modernized with regard electronic and computer control, at a heating rate of 20 K/min.

RESULTS

The mesophase content was found to affect the stress–strain curves for the PDES networks markedly. Furthermore, the networks contain different amounts of the mesophase depending on M_c and their thermal history. An accurate determination of the mesophase fraction in a PDES network especially near ambient temperature is, however, not straight forward due to the following reason. The isotropization temperatures of PDES networks are close to room temperature and to the temperatures of the antecedent α_2 and β_2 crystalline phases–mesophase transitions (280 and 290 K, respectively). As a result, the DSC procedure, which requires previous cooling of a sample, is only appropriate to determine accurately the overall amount of the mesophase that arises from the antecedent crystalline phases upon heating of the network. As reported earlier [8], the maximum overall content of crystalline α and β modifications, that is achieved upon slow cooling of the PDES networks, drops from approximately 0.9 to 0.3 with M_c decreasing from 115,000 to 22,000. Similarly, the content changes of the mesophase that forms in these semicrystalline networks upon heating above 260–280 K. As shown in Figure 1, the isotropization peak in the DSC trace

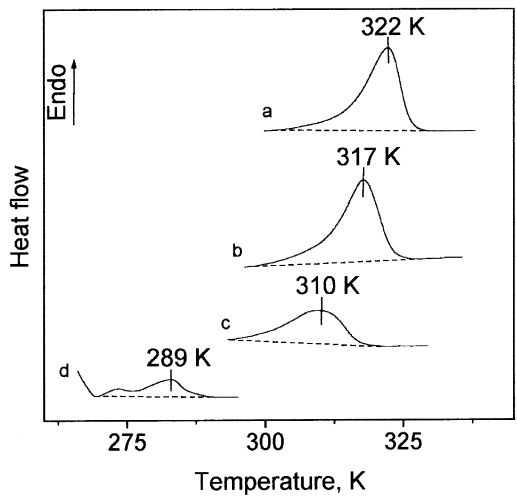

FIGURE 1 Segments of DCS traces for PDES-115 (a), PDES-94 (b), PDES-56 (c), PDES-22 (d) showing the temperature range of their isotropization (see full traces in Ref. [8]). Samples were previously cooled at a rate 10 K/min to 130 K. Heating rate 20 K/min.

of a PDES network extends over a temperature range of about 30 K. Its maximum shifts from 318 to 290 K as M_c diminishes from 115,000 to 22,000. In principle, one can also follow how the mesophase content in the network is changing in a dynamic regime of heating, based on the heat capicities in the DSC trace at various temperatures, but such estimated values can be different from those attained upon an isothermal storage of the network at the same temperatures.

Here we used X-ray diffraction data on the PDES networks in order to assess the mesophase content taking advantage of the different position of the mesomorphic reflection ($2\theta = 11.03°$) and amorphous halo (centered at $2\theta = 10.65°$) [13]. Samples were stored after preparation at ambient temperature without allowing them to crystallize by cooling to low temperatures. The X-ray diffractograms for PDES-94, PDES-56 and PDES-22 presented in Figure 2 demonstrate the phase changes with temperature. At ambient temperature the mesophase content in PDES-94 was rather high (≥ 0.8) and the mesophase disappeared completely only above 333 K. Crystallization of this network started on subsequent cooling to 273 K. For PDES-56 the mesophase content was estimated not to exceed 0.3 and full isotropization occurred above 303 K. PDES-22 was amorphous at 293 K and remained even so on cooling to 273 K. However, when this network was previously crystallized at low temperatures, DSC data demonstrated formation of a certain fraction of mesomorphic PDES upon heating the sample to ambient temperature.

Figure 3 illustrates the effect of the mesophase content on stress–strain curves (nominal stress (σ) *vs.* extension ratio (λ) plots) for PDES-115, PDES-94 and PDES-56. The stress–strain curves for PDES-115 and PDES-94 look similar to those observed on cold drawing of semi-crystalline polymers when necking occurs. The ultimate λ for both these networks was about 7 and after releasing the stress they contracted only slightly. The higher yield point for PDES-115 reflects a higher mesophase content in this network. The more complicated shape of the stress–strain curve for mesomorphic PDES-56 results from both the orientation of the originally existing mesophase domains and the increase of mesophase content during extension.

All investigated PDES networks could be converted to the amorphous state upon heating. Thus, the stress-induced formation of the mesophase could be observed by carrying out extension experiments at an appropriate temperature. Unstrained PDES-56, PDES-9 m and PDES-5 m displayed no evidence of the formation of mesocrystals at room temperature during very long time after previous heating to 353 K. Formation of the mesophase was however monitored clearly, when the samples were extended at ambient temperature. At this temperature the stress–strain curves for the PDES-56 and the bimodal PDES-9 m and PDES-5m were found to coincide up to $\lambda \cong 4$. Stress–strain curves for PDES-9m measured at three different strain rates

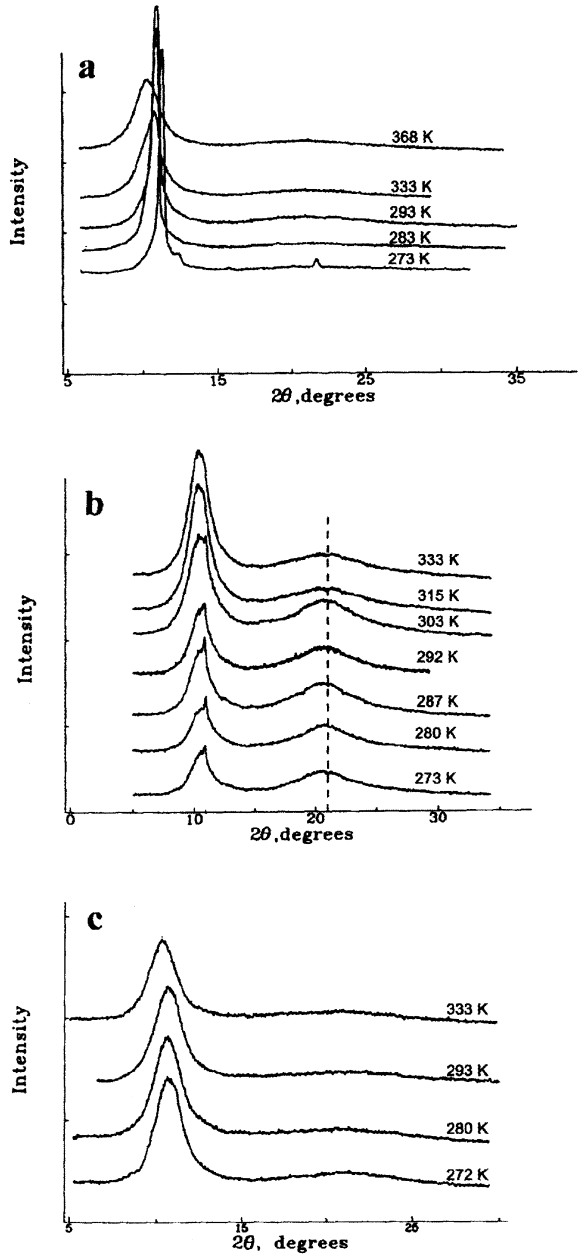

FIGURE 2 X-ray diffractograms for PDES-94 (a), PDES-56 (b) and PDES-22 (c) at different temperatures.

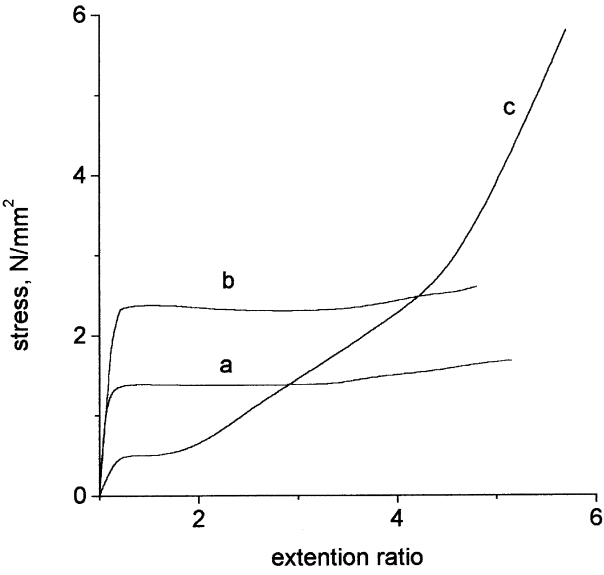

FIGURE 3 Stress–strain curves for mesomorphic PDES-115 (a), PDES-94 (b) and PDES-56 (c) taken at 293 K. Strain rate is 0.045 min^{-1}.

are depicted in Figure 4. These curves resemble those reported earlier for the slightly crosslinked PDES networks prepared by peroxide vulcanization [5].

The stress–strain curve in Figure 4 can be divided in four regimes. The first one extends up to $\lambda \cong 1.55-2.4$ depending on strain rate. At this section the real stress $\sigma_r = \sigma\lambda$ (applied force per unit cross-sectional area of the deformed sample) is almost linear with regard to strain, the strain is completely reversible and practically no stress hysteresis is observed on contraction (see Fig. 5, unloading from point A). The second rather short section is characterized by an approximately constant stress and relates to the initial stage of the mesophase formation evidenced by a sharp increase in birefringence (see Fig. 4). The elongation at constant stress produces about half the s-shape jump of birefringence caused by the mesophase formation. Upon stress relief from λ-values in the range of the plateau a stress hysteresis was observed due to a delayed contraction to the original length. Eventually, the extended networks contract completely (see Fig. 5, unloading from point B) and this means that the mesophase domains, formed during the previous extension, melt without constraint.

The position of the second section of the stress–strain curve on the extension ratio axis and the stress corresponding to the onset of the mesophase formation were strongly affected by strain rate and temperature. As shown in Figure 4, at strain rates of 0.5, 0.1 and 0.005 min^{-1} the

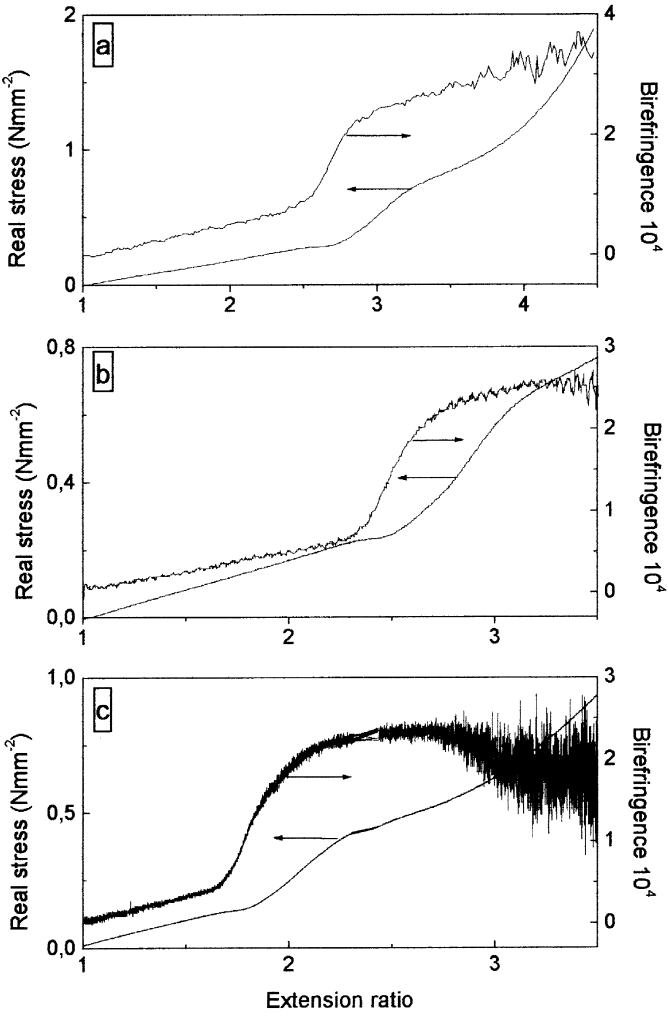

FIGURE 4 Combined plots real stress/birefringence *vs.* strain for amorphous PDES-9m. Strain rate: 0.5 min^{-1} (a), 0.1 min^{-1} (b) and 0.005 min^{-1} (c).

mesophase started to form at a real stress equal to 0.26, 0.21 and 0.13 N/mm^2 and the second section extended over strain ranges 2.45–2.7, 2.25–2.50 and 1.55–1.80, respectively. Raising the temperature increased the stress necessary to induce the mesophase formation. Figure 6 demonstrates stress-induced mesophase formation in PDES-56 at temperatures 293, 306 and 315 K at a strain rate of 0.5 min^{-1}. The onset of the mesophase formation occurred in the vicinity of $\lambda = 2.45$, 3.0 and 3.7 and the nominal stress equal to 0.11, 0.135 and 0.155 N/mm^2 respectively.

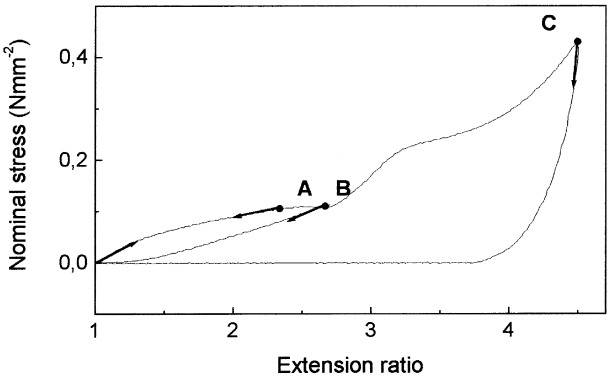

FIGURE 5 Stress–strain curves for amorphous PDES-56 taken at 293 K on extension and subsequent contraction from various extension ratios corresponding to different extension stages: reversible strain (A); after a partial formation of the mesophase at the second section of the stress–strain curve (B); ultimately stretched sample (C). Strain rate is 0.5 min^{-1}.

The third section in the stress–strain curve is manifested as a rather steep upturn of stress after which it is leveling off. It apparently reflects the final stage of the mesophase formation including also reorganization and re-orientation of the mesocrystals developed at lower extension ratios. The extension at this section is accompanied by the second part of the jumpwise increase in birefringence on the birefringence-strain curve. Irrespective of strain rate the overall increase in birefringence at the second and third sections of extension was about 2 10^{-4} at ambient temperature. At higher temperature the increase became larger and at 315 K it attained a value of about 4 10^{-4} as shown in Figure 7 where the birefringence is presented as a function of real stress.

The final, fourth section of the stress–strain curves is characterized by a sharp increase in stress and related to the stretching of the oriented yet-mesomorphic networks. The birefringence at this section seems to increase approximately linearly with extension ratio but precise measurement of its value was complicated by light scattering due to optical heterogeneity of the networks containing oriented fibril-like mesomorphic domains.

We failed to follow any stress-induced mesophase formation in the amorphous PDES-22 at ambient temperature due to its rupture at relatively small extension ratios. However, four sections stress–strain curves similar to those discussed above could be monitored for this network at lower temperatures (see Fig. 8a). For PDES-94, which was mesomorphic at ambient temperature, stress-induced mesophase formation could be observed at temperatures above 300 K provided the network samples were previously isotropized at 353 K. Figure 8b furnishes two stress–strain

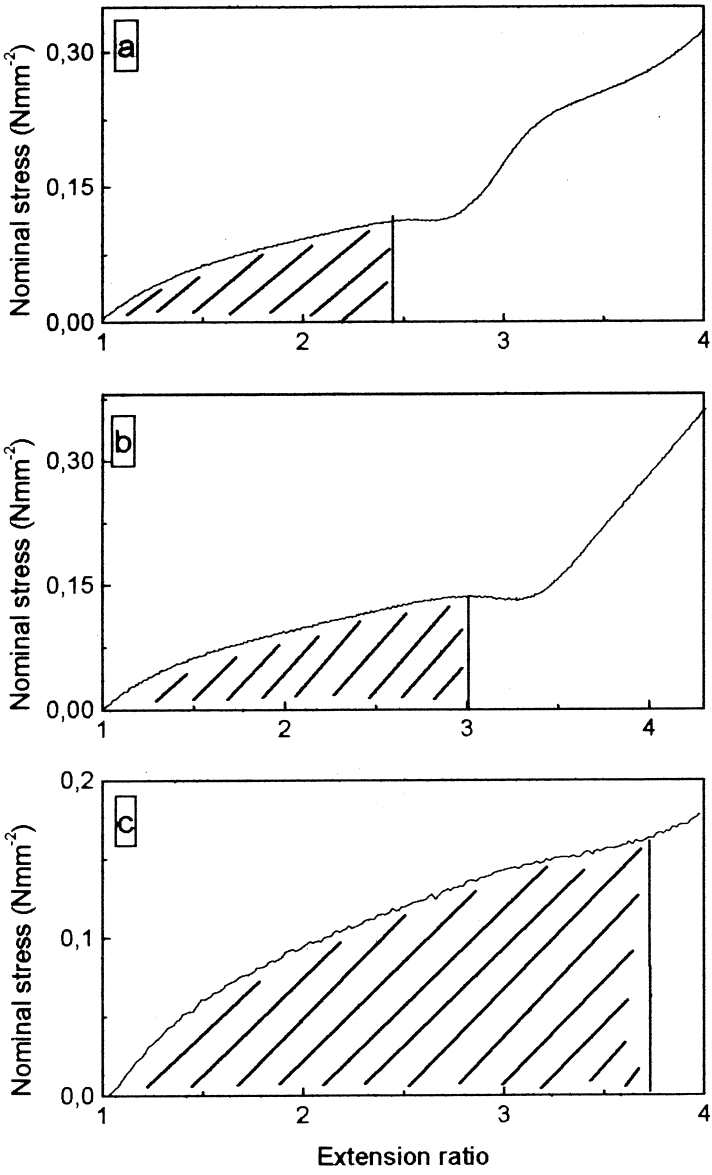

FIGURE 6 Stress–strain for amorphous PDES-56 at 293 K (a), 306 K (b) and 315 K (c). Strain rate is 0.5 min^{-1}. The hatched area under the first section of the curves corresponds to the work W required for deforming the network to extension ratio, at which stress-induced mesocrystals begin to form (see text and Eq. (8)).

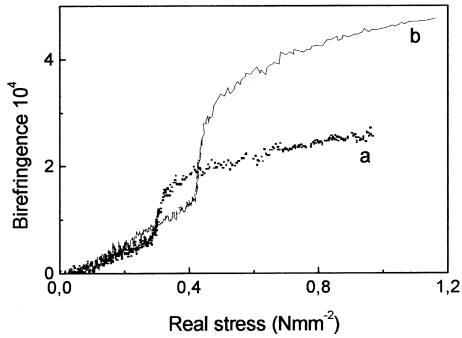

FIGURE 7 Birefringence as a function of real stress for PDES-56 at 293 K (a) and 306 K (b).

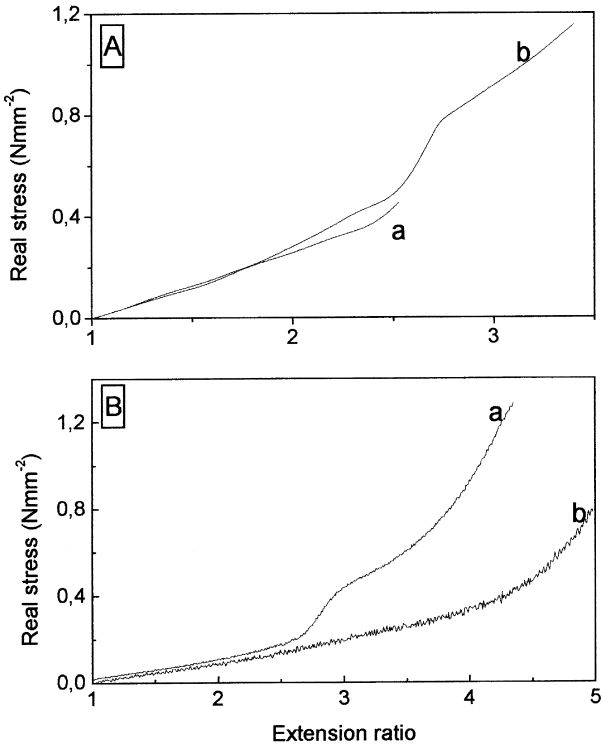

FIGURE 8 Stress–strain curves for PDES-22 and PDES-94 at different temperatures. A: PDES-22 at 293 K (a) and 283 K (b); strain rates are 0.015 min^{-1} (a) and 0.045 min^{-1} (b). B: PDES-94 at 303 K (a) and 314 K (b); strain rate is 0.25 min^{-1}.

curves for PDES-94 taken at 303 and 314 K. At the former temperature the onset of the mesophase formation occurs at $\lambda = 2.6$ and the extension curve also displays the four sections. At 314 K there is no well-defined second section and the mesophase begins to arise in the vicinity $\lambda = 4.2$ when the stress upturn is observed.

Along with the above measurements, that demonstrated the influence of temperature and strain rate on the mesophase formation upon extension of amorphous PDES networks with a different M_c, we investigated also the isotropization temperatures of stained mesomorphic samples when they are heated with fixed ends. It is obvious that in this case reliable T_i-stress relationships can be received only if such constrained samples are compared, which contain mesocrystals of a similar size. In order to meet this requirement we carried out our experiments in the following way. Samples of PDES-115, PDES-94 and PDES-56 were extended at ambient temperature to an extension ratio close to ultimate and kept under stress for some days. It was assumed that under such conditions most mesomorphic domains would attain their maximum size and perfection, *i.e.*, 'equilibrium' mesocrystals would form that cannot grow further upon additional strain. Elongation of these oriented mesomorphic samples was reversible and characterized by a very sharp increase in stress.

Stress relaxation for different original stresses and the changes in the intensity of the mesomorphic X-ray reflection (at $2\Theta = 11.03°$, see also Fig. 2) were monitored upon heating. We anticipated that the isotropization of the mesomorphic domains should lead to an increase in stress due to the entropic retractive force of the extended chains converted into amorphous state. However, only for PDES-56 we could observe such a well-defined increase in the stress (see Fig. 9). Furthermore, the constrained networks were found to display rather complicated stress relaxation upon heating. The increase in stress was always preceded by a considerable one- or two-stage stress relaxation. X-ray diffraction showed that the upturn in the stress – temperature curve corresponds to the complete isotropization of the sample. The insert in Figure 9 depicts the relative intensity of the mesomorphic equatorial X-ray reflection as a function of temperature for the most constrained sample. On heating the reflection intensity diminishes and approaches zero at about 333 K. Consequently, we have taken the temperatures related to the onset of the stress increase as the end point of istropization at the corresponding stress (indicated by the horizontal bars in Fig. 9) For constrained oriented samples of PDES-115 and PDES-94 we could not observe an increase in stress upon heating. At higher applied stresses, the samples broke before isotropization; at lower stresses only the plateau was reached after an initial relaxation. Upon subsequent cooling the stress remained unchanged or decreased a little further. Concurrently, the intensity of the mesomorphic reflection in the X-ray diffractogram,

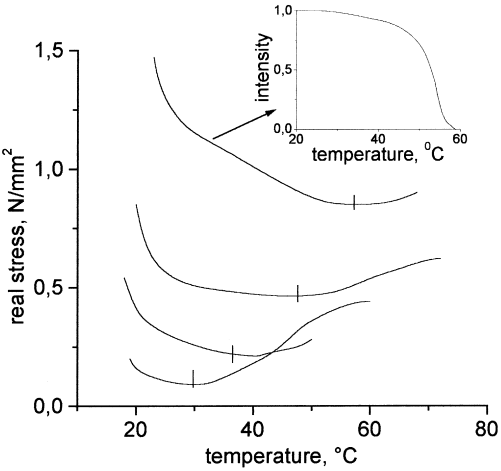

FIGURE 9 Changes in stress upon heating in previously oriented mesomorphic samples of PDES-56 to which different initial stress were applied (see text). Heating rate is 2 K/min. The insertion at the upper right shows the relative intensity of mesomorphic interchain reflection at $2\Theta = 11.03°$ as a function of temperature for the sample under the highest initial stress.

which had dropped to zero upon heating, reestablished completely pointing to the formation of a highly oriented mesophase superstructure.

DISCUSSION

Reversible Deformation

Within the first section of the stress–strain curve all PDES networks in the amorphous state display rubber elasticity, *i.e.*, the deformation is reversible and mechanical hysteresis upon unloading is practically absent. Therefore, we have determined the initial modulus of elasticity E of the networks at 323 K, by indentation, by a more detailed characterization of their structure. It was found to be equal to 51, 84 164 and 120 kPa for PDES-94, PDES-56, PDES-22 and PDES-9m, respectively. Using these values and Eq. (2) obtained from rubber elasticity theory [14], one can estimate the elastically effective network strand M_c between crosslinks with ρ representing the network density and R being the gas constant:

$$M_c = 3\rho RT/E \tag{2}$$

The obtained values of M_c (53000, 31300, 17200 and 21400 g mol^{-1} for PDES-94, PDES-56, PDES-22 and PDES-9m) proved to be markedly lower than those expected from MW of the original telechelics and indicated in Experimental section. This fact implies that the use of the multifunctional

cross-linking agents lead to a complicated topology of the networks, *i.e.*, to the occurence of chain entanglements which contribute to the elastic modulus. Note in this connection that such a situation is rather common for different end-linked network of high functionalities and this problem has been not unequivocally resolved [15].

Within the first stage of extension of these PDES networks, the real stress σ_r is practically linear with strain (see Figs. 6 and 7) and can formally be described by the equation:

$$\sigma_r = \sigma\lambda = A(\lambda - 1) \tag{3}$$

where A is an elasticity coefficient which was estimated equal to 0.18 MPa for PDES-56, PDES-9m and PDES-5m and 0.24 MPa for PDES-22 at 293 K. Upon raising the temperature from 293 to 315 K the value of A for the first three networks increases slightly up to 0.20 MPa as it is expected for entropic elasticity. For amorphous PDES-94 at 314 K the value of A was found to be 0.09 MPa. Thus, the elasticity coefficient increases with decreasing M_c, however, no analytical relationship between these parameters can be proposed.

The coincidence of the stress–strain curves for PDES-56, PDES-9m and PDES-5m is surprising regarding that the average molecular weights between crosslinks is quite different. This might be seen as an indication that even relatively small strains induce some ordering of the PDES chains that obliterates the rubber elasticity dependence on the M_c of the networks. A more detailed consideration of the rubber elasticity of swollen networks in various solvents and dry PDES networks will be published separately.

Birefringence

In the first regime, the birefringence Δn of the amorphous PDES networks is a linear function of the real stress σ in accordance with the well-known relationship for elastomeric networks where B is the stress-optical coefficient [16]:

$$\Delta n = B\sigma \tag{4}$$

The values of B were found to be positive and rather similar for all amorphous PDES networks, *i.e.* $(2.8 \pm 0.2) \cdot 10^{-4}$ and $(2.5 \pm 0.2) \cdot 10^{-4}$ mm^2/N for PDES-56 and PDES-22 respectively at 293 K. The stress optical coefficient is related to the anisotropy of the polarizability of the optical Kuhn's segment $\Delta\alpha$ through the expression:

$$B = 2\pi\Delta\alpha/45\,kT[(n^2 + 2)^2/n] \tag{5}$$

where n is the refractive index of non-deformed sample [16]. Taking n of the PDES networks equal to the refractive index of a high molecular weight

linear PDES (1.452 at 298 K for white light), we estimated the average of $\Delta\alpha$ for them to be $6.6 \cdot 10^{-25}\,cm^3$. This value is somewhat higher than $\Delta\alpha = 4.7 \cdot 10^{-25}\,cm^3$ reported for polydimethylsiloxane (PDMS) [17].

In the temperature range from 293 to 306 K the value of B remains practically unchanged whereas the overall jumpwise increase in birefringence due to the stress-induced formation of the mesophase is by a factor of ~ 1.5 larger at 306 K than that at 293 K (see Fig. 7). According to calorimetric data reported earlier for peroxide crosslinked PDES networks [5], the limiting mesophase content attained on extension decreased with increasing temperature. To explain this discrepancy, we compared the optical anisotropy Δa of the monomer unit $-(C_2H_5)_2SiO-$ in the mesomorphic and amorphous state of the PDES macromolecule. In the former case Δa_m can be estimated assuming a cylindrical symmetry of the mesophase domains and using a simplified relationship derived for crystals with an axially symmetrical ellipsoid of polarizability [16]

$$4/3\pi N\Delta a \cong 6n\Delta n/(n^2+2) \quad (\text{if}\Delta n \ll n) \tag{6}$$

where Δn is the difference between refractive indices parallel and perpendicular to the macromolecular axis and N presents the number of the monomer units per cm^3. Taking the average refractive index n for mesomorphic PDES equal to that of amorphous PDES and assuming that Δn for the mesocrystal cannot exceed $4 \cdot 10^{-4}$ at ambient temperature (see ultimate values of Δn in Figs. 4 and 7) one arrives at a marginal value of $\Delta a_m \cong 8 \cdot 10^{-27}\,cm^3$. The optical anisotropy of the monomer unit for amorphous PDES macromolecules Δa_a can be calculated from the anisotropy of polarizability of the optical Kuhn's segment $\Delta\alpha$ if the number of monomer units comprising the segment is known. Based on the similar molecular flexibility of PDMS and PDES [18], it can be assumed that the latter does not exceed considerably the value for PDMS. The optical Kuhn's segment of the PDMS macromolecule contains five monomer units [17]. If the Kuhn's segment of the PDES is assumed to consist of seven $(C_2H_5)_2SiO$-units, Δa_a results to be $\sim 9\ 10^{-26}\,cm^3$, *i.e.*, about one order of magnitude higher than Δa_m. Such a large difference in the values of Δa for amorphous and mesomorphic PDES macromolecules must be caused by varying contributions of ethyl groups to the overall optical anisotropy of the $(C_2H_5)_2SiO$-units. The difference between the polarizabilities parallel and perpendicular to a C—C bond is rather high and the contribution to the optical anisotropy by the ethyl side groups will depend strongly on the conformation of the Si—C bonds in the $CH_3—CH_2—Si—CH_2—CH_3$ units. Orientation of the ethyl groups towards the —Si—O— backbone and the conformational mobility, however, varies with the phase state and temperature. According to Ref. [19], the birefringence is negative for a stretched crystalline PDES film and becomes positive when the temperature is raised after the transition into the

mesomorphic state. Consistent with NMR studies on the molecular mobility and conformational order [20–22], it can be concluded that the average orientation of the ethyl side chains towards the fiber axis in the mesophase is gradually broadening with temperature. Consequently, the temperature dependent increase in birefringence of the strain induced mesophase of a PDES rubber can be explained by the growth of the positive optical anisotropy of the $(C_2H_5)_2SiO$-units with temperature in the mesomorphic state.

Thermodynamic and Kinetic Aspects of the Mesophase Formation

In accordance with rubber elasticity theory [23] and similar to the melting of strained crystalline rubbers, the isotropization temperature T_i of a uniaxially deformed PDES network should increase with increasing applied force f:

$$dT_i/df = \Delta l/\Delta S \tag{7}$$

where Δl and ΔS are in this case the changes in the length and entropy on fusion of a deformed network. In the strict sense this equation relates to T_i of mesocrystals of infinite size or similar sizes at different f. However, under real conditions it must be taken into account that mesocrystals of different sizes are formed even in the same network.

As shown in Figure 1, T_i increases with increasing M_c when the mesocrystals have been formed in an unconstrained PDES network upon slow cooling. According to Ref. [8], extrapolation of these T_i for infinite M_c yields a value of $T_i = 331\,K$ consistent with the value proposed for linear PDES with infinite molecular weight. This implies that the chains in the mesocrystals are extended and the ultimate size of most mesocrystals in the networks is thus determined by the molecular weight of chains between the chemical crosslinks, M_c, despite the existence of chain entanglements (see Section "Revesible deformation"). Such mesocrystals can be regarded to approach the equilibrium state for a given M_c and should form in particular at very low strain rates and maximum extension ratios.

If one considers for the sake of simplicity that T_i depends linearly on the applied stress, one can depict the stress dependence of the isotropization/formation of such 'equilibrium' strain-induced mesocrystals in PDES networks for different M_c as it is shown in Figure 10. In this graph T_i^1, $T_i^2, \ldots, T_i^{inf}$ on the ordinate axis designate the isotropization temperatures at stress $\sigma = 0$ for the mesocrystals of 'equilibrium' sizes l_1, $l_2, \ldots, l_{inf}$ which correspond to $M_c = M_c^1, M_c^2, \ldots, M_c^{inf}$. Two dashed horizontal lines indicate two temperatures at which the networks are stretched ($T_1 < T_2$). The diagram demonstrates that the stress, that is needed for the formation of 'equilibrium' mesocrystals of sizes l_1, l_2 and l_3, is the higher the smaller M_c ($\sigma_d > \sigma_c > \sigma_a$). When a particular network is extended at different

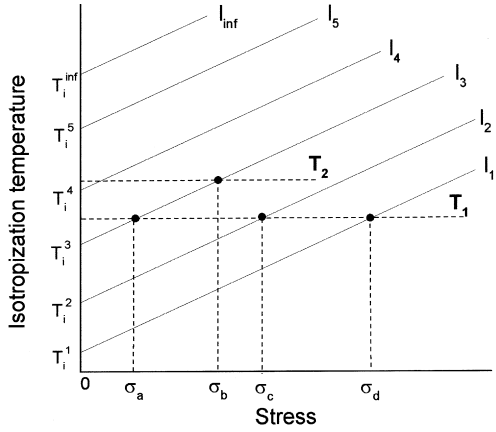

FIGURE 10 Schematic diagram of the dependence of isotropization temperature T_i on stress σ for mesocrystals of various size l_n corresponding to different M_c^n in PDES networks. $l_1(M_c^1) < l_2(M_c^2) < l_3(M_c^3), \ldots, < l_{inf}(M^{inf})$.

temperatures T_1 and T_2, the stress, at which the 'equilibrium' mesocrystals can exist, increases with increasing temperature ($\sigma_b > \sigma_a$). The data on the isotropization of the strained PDES-56 sample (Fig. 10) are in good agreement with this evaluation. A plot of T_i *versus* the monitored real stress for this network is presented in Figure 11. The points can be approximated by

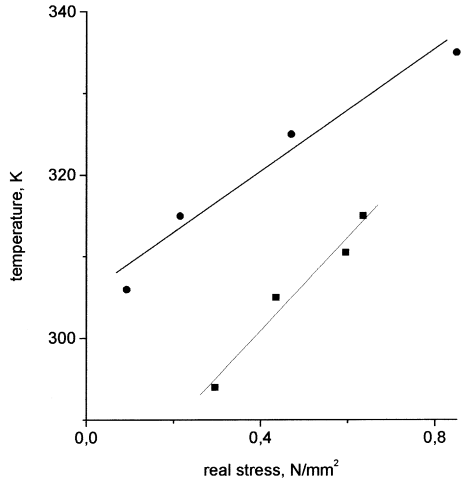

FIGURE 11 Isotropization temperature T_i as a function of stress for PDES-56: (●) data for previously oriented mesomorphic samples (taken from Figure 8); (■) data from stress–strain curves taken at different temperatures (see Figure 5 and text).

a straight line that extrapolates at $\sigma = 0$ to $T_i = 306\,K$. This value is close to $T_i = 310\,K$ observed for the slowly cooled sample of PDES-56 in quiescent state (see Fig. 1), *i.e.*, for the 'equilibrium' mesocrystals.

At the experimental strain rates, the mesocrystals grown first at the second stage of extension are smaller than the "equilibrium" size. At this stage, strain induced mesocrystal formation always occurred at temperatures below T_i for the 'equilibrium' mesocrystals and melted upon subsequent unloading with full contraction of the sample (see Fig. 5). Therefore, the temperatures, at which the samples were extended, can be taken for T_i of such nonequilibrium mesocrystals and correlated with the approximately constant stress during the second stage of extension when about half the total transformation takes place. Figure 11 represents a plot of these isotropization temperatures *versus* the real stress based on the data from Figure 6. Linear extrapolation to $\sigma = 0$ yields $T_i = 278\,K$. If the size of the mesocrystals formed upon strain is assumed to be independent of the temperature, this extrapolated value can be regarded as the isotropization temperature of such crystals in the quiescent state.

An alternative, eventually superior approach to evaluate T_i^0 at zero strain for the stress-induced mesocrystals at $\sigma = 0$ is based on the equation connecting the melting point of crystals in uniaxially deformed elastomers with the free enthalpy change of amorphous chains upon extension [21]. In our case this equation can be rewritten as

$$1/T_i = 1/T_i^0 - (1/T_i \Delta H_i) \int_1^\lambda \sigma(\lambda, T_i) d\lambda = 1/T_i^0 - (1/T_i \Delta H_i) W \qquad (8)$$

where T_i^0 is the isotropization temperature of mesocrystals in a non-deformed network, ΔH_i is the specific heat of isotropization, and σ presents the nominal stress. The integral in the second term in the right-hand side of Eq. (8) describes the work W required for deforming the network to extension ratio λ, at which stress-induced mesocrystals begin to form. This λ corresponds to the onset of the second section of the stress–strain curve. If Eq. (8) is applicable, a linear dependence between $1/T_i$ and W/T_i is expected with a slope determined by the heat of isotropization. Such a plot is shown in Figure 12 for PDES-9m. The values of W were calculated from the area under the first section of the stress–strain curves in Figure 6 (the hatched area). According to the slope of the line, $\Delta H_i = 2.5\,J/g$ that is in a quite good agreement with $\Delta H_i = 3\,J/g$ reported for linear PDES [2, 19]. The intercept at $W/T_i = 0$ yields a value of $T_i^0 = 283\,K$ which is very close to $T_i^0 = 278\,K$ obtained above. The coincidence of these results supports the assumption that rather similar populations of mesocrystals formed on extension of PDES-56 networks at different temperatures with $T_i^0 \sim 280\,K$ at $\sigma = 0$. This value of T_i^0 for nonequilibrium mesocrystals can be used to estimate their sizes by comparison with T_i of the 'equilibrium' mesocrystals in

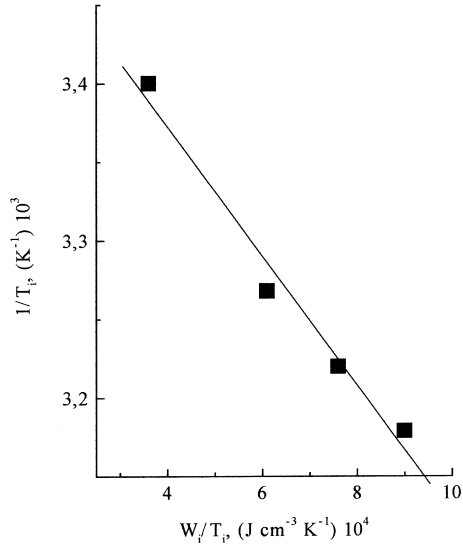

FIGURE 12 Plot of reciprocal isotropization temperature T_i *versus* W/T_i (see text and Eq. (8)).

unconstrained PDES networks with different M_c. The above value of T_i^0 is considerably less than T_i^0 of the 'equilibrium' mesocrystals for the PDES-56 (310 K) but close to that observed for PDES-22 (289 K). This implies that on extension of PDES-56 nonequilibrium mesocrystals formed whose size likely was close to that of the 'equilibrium' mesocrystals in PDES-22.

The formation of nonequilibrium mesocrystals implies that the transition of amorphous PDES chains into the mesomorphic state upon extension is controlled not only by thermodynamic but kinetic factors as well. Nucleation and subsequent growth of mesocrystals proceeds not instantly. As a result, at any experimentally reasonable strain rate the mesophase formation can be observed only at a stress that is higher than the stress required for 'equilibrium' mesocrystals of a given network at the temperature of extension. Regarding the data in Figure 10, it follows that for the extension of a network with M_c^3 the onset of mesophase formation can be only observed if the stress higher than σ_a is acheived, at which 'equilibrium' mesocrystals of the size l_3 are stable. The number of critical mesophase nuclei should be an essential factor for the overall growth rate of each population of mesocrystals at a given temperature and λ. The formation rate of the nuclei of each size is, however, expected to increase with increasing extension ratio, the number of nuclei of a smaller size being larger than those of a larger size at every λ. Therefore, the overall growth rate for

mesocrystals of various sizes, which are stable at a given stress, should differ in much the same fashion.

If we assume that the stress dependence of T_i for nonequilibrium mesocrystals of different size l_i is similar to that shown in Figure 10 for the 'equilibrium' mesocrystals ones, we can consider the extension of the network with M_c^3 at temperature T_1 with an experimentally reasonable strain rate v_1 in more detail. At the extension ratio corresponding to σ_a, the number of critical nuclei would be too small to detect the formation of the mesophase experimentally. On further extension, corresponding to σ_d, nonequilibrium mesocrystals with a size of $l_1 < l_3$ become stable and the mesophase is formed at an appreciable rate as a sufficient number of critical nuclei will be present.

As can be seen in Figures 4 and 6, the onset of the mesophase formation manifests itself by a decrease of the slope of the stress–strain curve reaching a plateau in the second regime. This stress compensation effect may be explained by the incorporation and orientation of chains of the amorphous fraction into growing mesocrystals. Thus, strain induced mesophase formation was monitored directly and without delay as the strain rate became commensurate to the linear growth rate of the mesocrystals in the extension direction. Consequently, the linear growth rate in the second regime of the strain–stress curve can be taken equal to the strain rate in a first approximation.

As shown above (see Fig. 4), the stress and extension ratio at the onset of the mesophase formation are strongly affected by strain rate but the length of the second section of the stress–strain curve ($\Delta\lambda$) depends very slightly on strain rate varying from ~ 0.25 to 0.3. On the contrary, the duration (Δt) of the second section changes very strongly. For example, in the case of PDES-9m, Δt increases from 0.6 to 56 min when the strain rate decreases from 0.5 to 0.005 min^{-1}. As $\Delta\lambda$ is very small and the stress is practically constant, the formation of the mesophase at this stage of extension can be regarded to proceed at constant stress and constant λ. Consequently, Δt can be used as a parameter indicating how the stress and the extension ratio affect the kinetics of formation of the nonequilibrium mesocrystal populations. Referring again to the diagram in Figure 10, one can also conclude that at different strain rates mesocrystals of different sizes are expected to grow. For instance, on extension at a strain rate $v_2 < v_1$, nonequilibrium mesocrystals will start to form at a lower stress (say at $\sigma_c < \sigma_d$) and, consequently, their size should be larger than that at v_1 ($l_2 > l_1$). With increasing mesophase content in the course of extension, the influence of the mesocrystals, serving as physical crosslinks, becomes more and more pronounced and, eventually, the mesophase domains appear to merge into a continuous phase resulting in a change of the deformation mechanism. The occurrence of a third and fourth regime in the stress–strain

dependence reflects this change. Along with additional formation of nonequilibrium mesocrystals, reorganization and further orientation of mesocrystals formed before is supposed to cause the conversion to 'equilibrium' mesocrystals for a given M_c. The stress dependence of T_i for such mesocrystals has been considered above. If T_i of the formed 'equilibrium' mesocrystals is higher than the experimental temperature they do not melt after subsequent unloading and the extended network remains in the oriented mesomorphic state. Such a situation is observed when amorphous PDES-56, PDES-9m and PDES-5m are drawn at ambient temperature to λ values corresponding to the fourth section of the stress–strain curve (see Fig. 5, contraction from point C). Thus, both initially mesomorphic and initially amorphous PDES networks can be converted into a stable highly oriented mesomorphic state by extension up to limiting extension ratios (compare Figs. 3 and 5).

Unloading of a PDES network that has been originally amorphous and became mesomorphous upon extension at ambient temperature to a λ in the third regime of the strain–stress curve, leads to a peculiar relaxation behavior. Contraction proceeds first by formation of one or more isotropic segments of the rubber band with sharply defined boundaries towards the mesomorphic domains. These isotropic regions grow at the expense of the remaining oriented mesomorphic sections. Earlier we called this phenomenon "reverse necking" [5, 6]. In light of the above considerations it can be explained by the formation of mesocrystals whose isotropization temperature is very close to ambient temperature due to their small size. These mesocrystals melt on unloading. The strained chains in the thus formed amorphous domains will contribute to the stress on the oriented domains and the isotropization of the whole sample. Consequently the further contraction of the oriented sample (growth of the amorphous section) proceeds at constant stress. As the formation and reorganization of mesocrystals on extension are kinetically governed processes, the mesocrystals melting on unloading and reverse necking is strongly affected by extension and contraction rates.

CONCLUSIONS

Depending on the molecular weight between crosslinks M_c and the applied stress, PDES networks exist in the mesomorphic state in various temperature ranges. The behavior of mesocrystals under stress can in principle be described by the thermodynamic and kinetic relations derived for strain induced rubber crystallization. At the initial stage of extension and at experimentally reasonable strain rates, nonequilibrium mesocrystals with sizes smaller than M_c form, which melt after releasing the applied stress. On further extension, such mesocrystals can reorganize into "equilibrium" ones

whose ultimate longitudinal size and, consequently, isotropization temperature are determined by the M_c of each network. This is a peculiar feature of the mesophase formation in PDES networks, which differs this process from crystallization of rubbers under stress. It controls the stress–strain behavior on extension and subsequent contraction and suggests the development of elastomeric materials with specific viscoelastic properties.

The optical anisotropy of $(C_2H_5)_2SiO$ units of mesomorphic macromolecules was found to be considerably less than that in the amorphous state. This suggests that rotation of the side ethyl groups around Si—C bond in the mesophase remains restricted to a certain extent. Despite this fact, formation of the mesophase upon extension is accompanied by a jumpwise increase in positive birefringence. The increase can apparently be attributed to a high degree of orientations of the macromolecular chains in mesocrystals and the mesocrystals themselves along the extension direction.

REFERENCES

[1] Beatty, C. L., Pochan, J. M., Froix, M. F. and Hinman, D. D. (1975). *Macromolecules*, **8**, 547.
[2] Godovsky, Ju. K. and Papkov, V. S. (1989). *Adv. Polym. Sci.*, **88**, 129; (b) Godovsky, Yu. K., Papkov, V. S. Poly(diethylsiloxane), In: "*Polymer Data Handbook*", Ed. Mark, J. E., Oxford University Press, NY, 1999, p. 396.
[3] Ungar, G. (1993). *Polymer*, **34**, 2050.
[4] Moeller, M., Siffrin, S., Koegler, G. and Oelfin, D. (1990). Makromol. *Chem. Macromol. Symp.*, **34**, 171.
[5] Papkov, V. S., Godovsky, Ju. K. and Svistunov, V. S. (1989). *Vysokomol. Soed.*, **A31**, 1577.
[6] Papkov, V. S. and Kvachev, Ju. P. (1989). *Progr. Colloid. Polym. Sci.*, **80**, 221.
[7] Godovsky, Ju. K. and Valetskaya, L. A. (1991). *Polym. Bull.*, **27**, 187.
[8] Out, G. J. J., Turetskii, A. A., Snijder, M., Moeller, M. and Papkov, V. S. (1995). *Polymer*, **36**, 3213.
[9] Out, G. J. J., In: "*Poly(di-n-alkoxysiloxanes): Synthesis and Molecular Organization*", *Ph.D. Thesis*, University of Twente, The Netherlands, 1994.
[10] Aushra, C. and Stadler, R. (1993). *Macromolecules*, **26**, 6364.
[11] Abetz, V., Dardin, A., Stadler, R., Hellmann, J., Samulski, E. T. and Spiess, H. W. (1996), **274**, 723 1.
[12] Nielsen, L. E., "*Mechanical Properties of Polymer and Composites*", Marcel Dekker Inc., NY, 1974, Ch. 6.
[13] Tsvankin, D. Ja., Papkov, V. S., Zhukov, V. P., Godovsky, Ju. K., Svistunov, V. S. and Zhdanov, A. A. (1985). *J. Polym. Sci., Polym. Chem.*, **23**, 1043.
[14] Flory, P. J., "*Principles of Polymer Chemistry*", Cornell University Press, Ithaca, NY, 1953.
[15] Erman, B. and Mark, J. (1997). *Structures and Properties of Rubberlike Networks*, Oxford University Press, NY, pp. 134–143.

[16] Volkenstein, M. V. (1963). *Configurational Statistics of Polymeric Chains*, Wiley (Interscience), NY, Ch. 7.
[17] Tsvetkov, V. N. (1964). In: *Newer Methods of Polymer Characterization* (Ed. Ke, B.), Interscience Publishers, NY, Ch. XIV.
[18] Mark, J. E., Chin, D. S. and Su, T. K. (1978). *Polymer*, **19**, 407.
[19] Papkov, V. S., Svistunov, V. S., Godovsky, Ju. K. and Zhdanov, A. A. (1987). *J. Polym. Sci., Polym. Phys.*, **25**, 1859.
[20] Kögler, G., Hasenhindl, A. and Möller, M. (1989). *Macromolecules*, **22**, 4190–4196.
[21] Kögler, G., Loufakis, K. and Möller, M. (1990). *Polymer*, **31**, 1538–1545.
[22] Litvinov, V. M., Macho, V. and Spiess, H. W. (1997). *Acta Polymerica*, **48**, 471.
[23] Treloar, L. R. G., *The Physics of Rubber Elasticity*, Clarendon Press, Oxford, 1975.
[24] Krigbaum, W. R. and Roe, R.-J. (1964). *J. Polym. Sci.*, **A2**, 4391.